

Article

Dmisteinbergite, $\text{CaAl}_2\text{Si}_2\text{O}_8$, a Metastable Polymorph of Anorthite: Crystal-Structure and Raman Spectroscopic Study of the Holotype Specimen

Andrey A. Zolotarev ^{1,*} , Sergey V. Krivovichev ^{1,2} , Taras L. Panikorovskii ^{1,3} ,
Vladislav V. Gurzhiy ¹ , Vladimir N. Bocharov ⁴  and Mikhail A. Rassomakhin ⁵

¹ Department of Crystallography, Institute of Earth Sciences, St. Petersburg State University, University Emb. 7/9, 199034 St. Petersburg, Russia; s.krivovichev@spbu.ru (S.V.K.); taras.panikorovsky@spbu.ru (T.L.P.); vladislav.gurzhiy@spbu.ru (V.V.G.)

² Nanomaterials Research Centre, Kola Science Centre, Russian Academy of Sciences, Fersmana 14, 184209 Apatity, Russia

³ Laboratory of Nature-Inspired Technologies and Environmental Safety of the Arctic, Kola Science Centre, Russian Academy of Sciences, Fersmana 14, 184209 Apatity, Russia

⁴ Geo Environmental Centre “Geomodel”, Saint-Petersburg State University, Ul’yanovskaya Str. 1, 198504 St. Petersburg, Russia; bocharov@molsp.phys.spbu.ru

⁵ South Urals Federal Research Center of Mineralogy and Geoecology of UB RAS, 456317 Miass, Russia; miha_rassomahin@mail.ru

* Correspondence: a.zolotarev@spbu.ru or aazolotarev@gmail.com; Tel.: +7-812-350-66-88

Received: 29 August 2019; Accepted: 18 September 2019; Published: 20 September 2019



Abstract: The crystal structure of dmisteinbergite has been determined using crystals from the type locality in Kopeisk city, Chelyabinsk area, Southern Urals, Russia. The mineral is trigonal, with the following structure: $P312$, $a = 5.1123(2)$, $c = 14.7420(7)$ Å, $V = 333.67(3)$ Å³, $R_1 = 0.045$, for 762 unique observed reflections. The most intense bands of the Raman spectra at 327s, 439s, 892s, and 912s cm^{-1} correspond to different types of tetrahedral stretching vibrations: Si–O, Al–O, O–Si–O, and O–Al–O. The weak bands at 487w, 503w, and 801w cm^{-1} can be attributed to the valence and deformation modes of Si–O and Al–O bond vibrations in tetrahedra. The weak bands in the range of 70–200 cm^{-1} can be attributed to Ca–O bond vibrations or lattice modes. The crystal structure of dmisteinbergite is based upon double layers of six-membered rings of corner-sharing AlO_4 and SiO_4 tetrahedra. The obtained model shows an ordering of Al and Si over four distinct crystallographic sites with tetrahedral coordination, which is evident from the average $\langle T\text{--O} \rangle$ bond lengths (T = Al, Si), equal to 1.666, 1.713, 1.611, and 1.748 Å for T1, T2, T3, and T4, respectively. One of the oxygen sites (O4) is split, suggesting the existence of two possible conformations of the $[\text{Al}_2\text{Si}_2\text{O}_8]^{2-}$ layers, with different systems of ditrigonal distortions in the adjacent single layers. The observed disorder has a direct influence upon the geometry of the interlayer space and the coordination of the Ca2 site. Whereas the coordination of the Ca1 site is not influenced by the disorder and is trigonal antiprismatic (distorted octahedral), the coordination environment of the Ca2 site includes disordered O atoms and is either trigonal prismatic or trigonal antiprismatic. The observed structural features suggest the possible existence of different varieties of dmisteinbergite that may differ in: (i) degree of disorder of the Al/Si tetrahedral sites, with completely disordered structure having the $P6_3/mcm$ symmetry; (ii) degree of disorder of the O sites, which may have a direct influence on the coordination features of the Ca^{2+} cations; (iii) polytypic variations (different stacking sequences and layer shifts). The formation of dmisteinbergite is usually associated with metastable crystallization in both natural and synthetic systems, indicating the kinetic nature of this phase. Information-based complexity calculations indicate that the crystal structures of metastable $\text{CaAl}_2\text{Si}_2\text{O}_8$ polymorphs dmisteinbergite and svyatoslavite are structurally and topologically simpler than that of their stable

counterpart, anorthite, which is in good agreement with Goldsmith's simplicity principle and similar previous observations.

Keywords: dmisteinbergite; feldspar; polymorphism; metastability; burned coal dumps; Kopeisk; Ural region; crystal structure; Raman spectroscopy

1. Introduction

Feldspars are the most common rock-forming minerals of the Earth's crust, and constitute more than 50% of the continental crust [1]. Recent investigations revealed the existence of a number of metastable feldspar polymorphs in relevant melt inclusions [2–5], meteorites [6–9], high-pressure and ultra-high-pressure rocks [10–16], pyrometamorphic formations [17], and pseudotachylytes [18–20]. Similar to rock-forming feldspars, these metastable phases are based upon tetrahedrally coordinated Al^{3+} and Si^{4+} cations, but with drastically different structural topologies from the feldspar framework topology. Their formation can be explained using Goldsmith's principle of simplicity [21], which states that metastable kinetic mineral phases are structurally simpler than their stable thermodynamic counterparts. This principle, first formulated in 1953, was recently verified using information-based structural complexity measures and checked against mineral systems with different chemical compositions [22–28].

Metastable polymorphs with the composition $\text{CaAl}_2\text{Si}_2\text{O}_8$ (i.e., metastable polymorphs of anorthite) have been known for a long time [29–36]. There are at least two such polymorphs, sometimes described as “pseudo-orthorhombic” (or “monoclinic”) and “hexagonal” modifications. These are also known as the mineral species svyatoslavite [37,38] and dmisteinbergite [39,40], respectively, discovered in the burned coal dumps of the Chelyabinsk coal basin. It had been assumed that both svyatoslavite and dmisteinbergite crystallize directly from the gaseous phase under extreme reducing conditions at temperatures close to 1000 °C [41].

Dmisteinbergite is the so-called “hexagonal” polymorph of $\text{CaAl}_2\text{Si}_2\text{O}_8$, which was recently identified in a range of geological environments using scanning electron microscopy (SEM), electron backscattered diffraction (EBSD), and micro-Raman spectroscopy [6,8,9,18–20]. Its crystal structure model was originally reported in the $P6_3/mcm$ space group as having disordered arrangement of Si and Al atoms [30,36]. According to these studies, the structure of dmisteinbergite is based upon double layers of TO_4 tetrahedra (T = Si, Al), with Ca atoms in the interlayer space. However, the hexagonal symmetry of dmisteinbergite was questioned in the literature [32,42], due to its disagreement with observed X-ray powder diffraction patterns and the high degree of atomic disorder (the hexagonal model has only one symmetrically independent T site, which implies complete Al/Si disorder).

Herein, we report on the results of X-ray diffraction and Raman spectroscopic studies of dmisteinbergite from the holotype locality in the burned coal dumps, Kopeisk, Chelyabinsk region, Russia.

2. Materials and Methods

2.1. Materials

The sample of dmisteinbergite is a holotype sample (number 054-107) and was taken from the personal collection of B.V. Chesnokov. It is currently deposited at the Natural Science Museum of the Ilmen State Reserve (Miass, Russia). The sample originates from the coal dumps of mine number 45 near Kopeisk city, Chelyabinsk region, Southern Urals, Russia [41]. Dmisteinbergite and its orthorhombic polymorph svyatoslavite were found in the area containing “black blocks”, which are the products of extensive combustion of clays and carbonate rocks under reducing conditions at temperatures up to

1200 °C [39]. Dmisteinbergite was found as hexagonal platy crystals grown on the surface of charcoal (Figure 1).

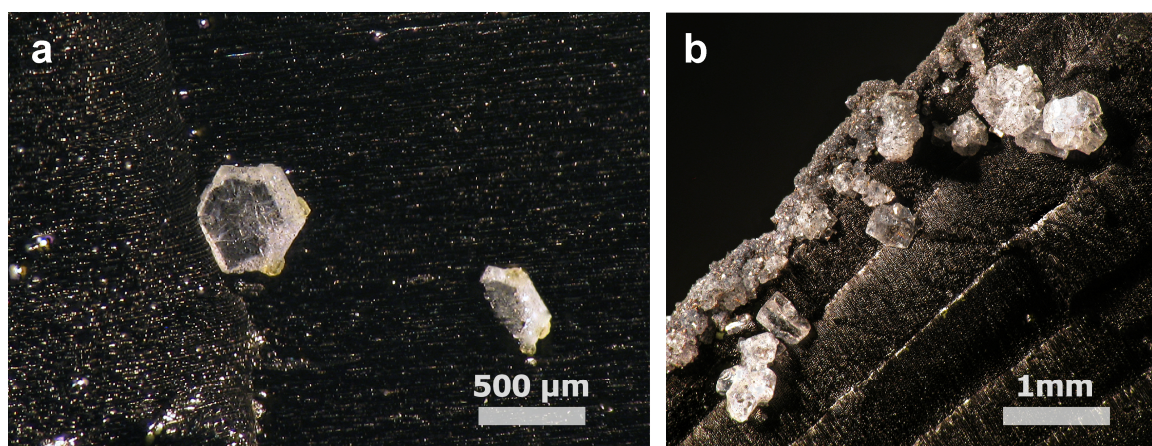


Figure 1. The crystals of $\text{CaAl}_2\text{Si}_2\text{O}_8$ polymorphs on the surface of charcoal: (a) hexagonal plates of dmisteinbergite; (b) dmisteinbergite in association with prismatic anorthite crystals. Photography by Gregory Yu Ivanyuk.

2.2. Single-Crystal X-ray Diffraction

Single-crystal X-ray diffraction study of dmisteinbergite was performed at the X-ray Diffraction Methods Resource Center of St. Petersburg State University using a Bruker Kappa APEX II DUO diffractometer operated at 45 kV and 0.6 mA (microfocus tube) and equipped with a CCD area detector. The study was done by means of monochromatic $\text{MoK}\alpha$ X-radiation ($\lambda = 0.71073 \text{ \AA}$), frame widths of 0.5° in ω , and with 10 s counting time for each frame. The intensity data were reduced and corrected for Lorentz, polarization, and background effects using the Bruker software APEX2 [43]. A semiempirical absorption correction based upon the intensities of equivalent reflections was applied using SADABS [44]. The unit cell parameters were refined by least square techniques using 2898 reflections. The structure was solved and refined in the space group $P312$ to $R_1 = 0.045$ ($wR_2 = 0.136$) for 703 unique observed reflections with $I \geq 2\sigma(I)$ using the ShelX program package [45] within the Olex2 shell [46]. The merohedral twinning model was introduced into the refinement at the later stage by applying the matrix $[100/010/00-1]$ with (001) as a twin plane. The resulting ratio of the two twin components was 0.51:0.49. During the refinement, a relatively large electron density peak was observed near the O4 atom, indicating splitting of this position into two sites. The splitting was modeled by introducing an additional O4A site with the O4–O4A distance of $1.13(1) \text{ \AA}$. The refinement of the occupancies of the split sites (constrained to be equal to 1) resulted in the site occupation factors of 0.60(1) and 0.40(1) for O4 and O4A, respectively. We note that no disorder of O sites was reported in the previous crystallographic works on dmisteinbergite [30,36]. Crystal data, data collection information, and refinement details are given in Table 1. Atom coordinates, site occupancies, and displacement parameters are listed in Table 2 and Table S1, whereas Table 3 contains selected interatomic distances. Table 4 provides the results of bond valence analysis with the bond valence parameters taken from a previous study [47].

Table 1. Crystal data and structure refinement for dmisteinbergite.

Crystal System	Trigonal
Space group	<i>P</i> 312
<i>a</i> , Å	5.1123 (2)
<i>c</i> , Å	14.7420 (7)
<i>V</i> , Å ³	333.67 (3)
<i>Z</i>	2
<i>D</i> _{calc} , g/cm ³	2.769
μ , mm ⁻¹	1.575
Crystal dimensions, mm	0.17 × 0.05 × 0.03
<i>F</i> (000)	276.0
Radiation	MoK α (λ = 0.71073)
2 θ range, degree	2.76–62.89
Index ranges	−7 ≤ <i>h</i> ≤ 7, −7 ≤ <i>k</i> ≤ 7, −21 ≤ <i>l</i> ≤ 16
Reflections collected	2731
Independent reflections	762 [<i>R</i> _{int} = 0.0198, <i>R</i> _{sigma} = 0.0189]
Data/restraints/parameters	762/0/48
Goodness of Fit	1.132
Final <i>R</i> indices [<i>I</i> ≥ 2 σ (<i>I</i>)]	<i>R</i> ₁ = 0.0451, <i>wR</i> ₂ = 0.1355
Final <i>R</i> indices [all data]	<i>R</i> ₁ = 0.0478, <i>wR</i> ₂ = 0.1382
Largest diff. peak/hole/eÅ ⁻³	0.57/−1.08

Table 2. Atomic coordinates, isotropic atom displacement parameters (Å²), and site-occupation factors (s.o.f.) for dmisteinbergite.

Atom	<i>x</i>	<i>y</i>	<i>z</i>	<i>U</i> _{eq}
Ca1	0	0	0	0.0099 (5)
Ca2	0	0	$\frac{1}{2}$	0.0154 (6)
T1	2/3	1/3	0.8622 (2)	0.0057 (6)
T2	1/3	2/3	0.8592 (3)	0.0114 (9)
T3	1/3	2/3	0.6358 (3)	0.0152 (9)
T4	2/3	1/3	0.6400 (3)	0.0066 (7)
O1	2/3	1/3	0.7536 (4)	0.013 (2)
O2	1/3	2/3	0.7460 (5)	0.021 (3)
O3	0.997 (1)	0.3821 (9)	0.9029 (2)	0.0055 (6)
O4 *	0.598 (2)	0.617 (2)	0.5964 (5)	0.017 (2)
O4A **	0.394 (3)	0.382 (3)	0.5967 (8)	0.019 (3)

Note: * s.o.f. = 0.60 (1), ** s.o.f. = 0.40 (1).

Table 3. Selected bond lengths (Å) in the crystal structure of dmisteinbergite.

T1–O1	1.600 (6)	T3–O2	1.625 (8)	T3–O2	1.625 (8)
T1–O3	1.688 (6) 3×	T3–O4	1.606 (9) 3×	T3–O4A	1.732 (19) 3×
<T1–O>	1.666	<T3–O>	1.611	<T3–O>	1.705
T2–O2	1.669 (10)	T4–O1	1.675 (8)	T4–O1	1.675 (8)
T2–O3	1.728 (6) 3×	T4–O4	1.773 (10) 3×	T4–O4A	1.66 (2) 3×
<T2–O>	1.713	<T4–O>	1.748	<T4–O>	1.664
Ca1–O3	2.429 (3) 6×	Ca2–O4	2.461 (7) 6×	Ca2–O4A	2.444 (10) 6×

Table 4. Bond-valence sums analysis (v.u. = valence units) for dmisteinbergite *.

Atom	T1	T2	T3	T4	Ca1	Ca2	Total
O1	1.07			0.94			2.01
O2		0.94	1.00				1.94
O3	0.84↓ ×3	0.81↓ ×3			0.29↓ ×6		1.94
O4			1.05↓ ×3	0.73↓ ×3		0.26↓ ×6	2.04
O4A			[0.75↓ ×3]	[0.98↓ ×3]		[0.28↓ ×6]	[2.01]
Total	3.58	3.38	4.15 [3.24]	3.12 [3.84]	1.73	1.57 [1.67]	

Note: * calculated using bond-valence parameters from a previous study [47]: T1–O and T3–O bonds (using Si–O parameters), T2–O and T4–O bonds (using Al–O parameters). The values given in square brackets [] are calculated for the occupied O4A site.

2.3. Raman Spectroscopy

Raman spectra of dmisteinbergite (Figure 2) were collected from the surfaces of hexagonal transparent plates at the Geomodel Resource Center of St. Petersburg State University using a Horiba Jobin-Yvon LabRam HR 800 system at room temperature using a 514 nm laser. The Raman spectra were recorded up to 1200 cm^{-1} . No peaks were observed in the region of 1200–4000 cm^{-1} .

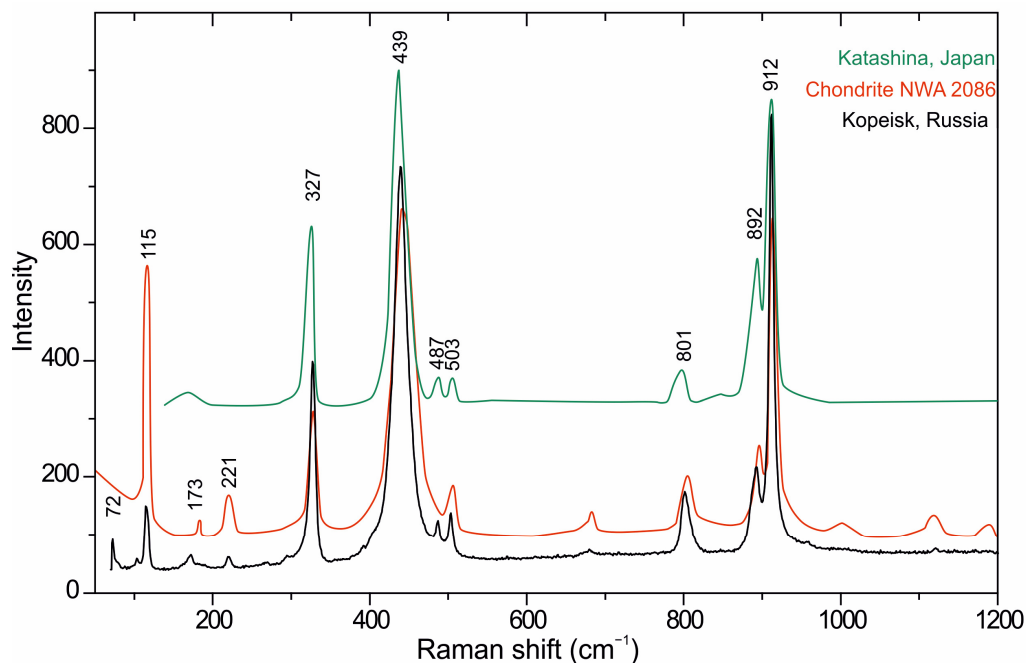


Figure 2. Raman spectrum of dmisteinbergite from Kopeisk (black) compared to the spectra obtained from the samples from Katashina village, Gunma Prefecture, Japan (green), and meteorite NWA 2086 (red).

3. Results

3.1. Raman Spectroscopy

The Raman spectrum of dmisteinbergite from the burned dumps of the Chelyabinsk coal basin is very similar to the published spectra of dmisteinbergite from the RRUFF Raman database [48] (Figure 2). The data were compared with the material from the deposit near Katashina village, Gunma Prefecture, Japan (RRUFF identification code R130087), and with the material from the meteorite NWA 2086 (RRUFF identification code R130085, museum of the University of Szeged, Hungary) [9].

At least six of the strongest bands in the region of 200–1200 cm^{-1} (327, 439, 503, 801, 892, and 912 cm^{-1}) match well in those dmisteinbergite spectra, and four bands (327, 439, 801, 912 cm^{-1})

match with dmisteinbergite from the Gole Larghe fault (Italian Alps) [18]. Interpretation of the bands present in the Raman spectra of dmisteinbergite is given in Table 5. The most intense bands at 327s, 439s, 892s, and 912s cm^{-1} correspond to the symmetric modes of stretching and bending vibrations in tetrahedra: Si–O, Al–O, O–Si–O, and O–Al–O [49]. The weak bands at 487w, 503w, and 801w cm^{-1} were attributed to the asymmetric stretching and deformation modes of Si–O and Al–O bond vibrations in tetrahedra. The weak bands in the range of 70–200 cm^{-1} can be attributed to Ca–O bond vibrations or lattice modes. The presence of additional bands in the spectra of sample NWA 2086 (1002w, 1122w, and 1194w cm^{-1}) and dmisteinbergite from the Chelyabinsk coal basin [40] (484s, 650s, and 935s cm^{-1}) are most likely due to the nano-sized (<1 μm) inclusions of quartz and anorthite.

Table 5. Raman shifts for the spectrum of dmisteinbergite *.

Shift, cm^{-1}	Vibration	Type of Vibration
912s, 892s, 801s	Si-O, Al-O	$\nu_{1,3}$
487w, 503w	O-Si-O, O-Al-O	ν_4
327s, 439s	Si-O, Al-O	ν_2
72w, 115w, 173w, 221w	Ca-O, lattice vibrations	T, ν_1

Note: * s—strong band, w—weak band.

3.2. Crystal Structure

The crystal structure of dmisteinbergite is based upon double layers of six-membered rings of corner-sharing AlO_4 and SiO_4 tetrahedra (Figure 3a). The high-symmetry $P6_3/mcm$ structure model for dmisteinbergite (“hexagonal anorthite”), which was previously reported [30,36], implies completely disordered distribution of Si and Al over one crystallographically independent tetrahedral site. In contrast, our model obtained in the space group $P312$ shows at least partial order of Al and Si over four distinct crystallographic sites with tetrahedral coordination. The existence of order is evident from the average $\langle T\text{-O} \rangle$ bond lengths ($T = \text{Al, Si}$), which are equal to 1.666, 1.713, 1.611, and 1.748 Å for T1, T2, T3, and T4, respectively. Therefore, T1 and T3 sites are predominantly occupied by Si, whereas the T2 and T4 sites are predominantly occupied by Al. The $P6_3/mcm$ structure model was first determined by Takeuchi and Donnay in 1959 [30] and refined to the essentially high crystallographic agreement index $R_1 = 13.8\%$. Dimitrijević et al. [36] refined the structure from the powder diffraction data using the Rietveld method and obtained the final agreement factors $R_p = 8.99\%$, $R_{wp} = 11.87\%$, and $R_B = 4.31\%$. The refinement was done using the model of Takeuchi and Donnay [30] from the mixture of dmisteinbergite and anorthite with the ratio 30:70% obtained by annealing Ca-LTA zeolite over 900 °C. The authors pointed out that the anorthite phase was of pure crystallinity, which increased the number of additional diffraction peaks and created considerable problems when refining the profile parameters. Under further annealing, the mixture transformed into pure anorthite, indicating the metastable character of dmisteinbergite. Considering the abovementioned problems in the previous studies, we believe that the $P312$ model is probably more correct, considering its general agreement with the basic crystal chemical principles, such as ordered arrangement of Al and Si atoms over tetrahedral sites.

The suggested splitting of the O4 site in dmisteinbergite implies the existence of two possible conformations of the $[\text{Al}_2\text{Si}_2\text{O}_8]^{2-}$ layers. The nature of the conformation can be described by the in-plane rotation of tetrahedra around the c axis. This phenomenon is well-known and has been studied in detail for minerals of the mica group [50,51]. The ideal tetrahedral layer formed by a six-membered ring has a hexagonal symmetry, with basal O atoms forming perfect hexagonal rings. The layers are actually distorted according to a ditrigonal rotation, which is defined as a rotation of tetrahedra around the axis perpendicular to the plane of the layer (Figure 4). The degree of the distortion is specified by the tetrahedral rotation angle α , which in dmisteinbergite is 22.1°. The directions of ditrigonal rotation in two adjacent layers comprising a double layer may be either identical (++ or --) or opposite (+– or –+). The former case is realized when the O4 site is occupied, and therefore, the layers have the

configuration shown in Figure 3b. The latter case is realized when the O4A site is occupied and the O4 site is vacant (Figure 3c).

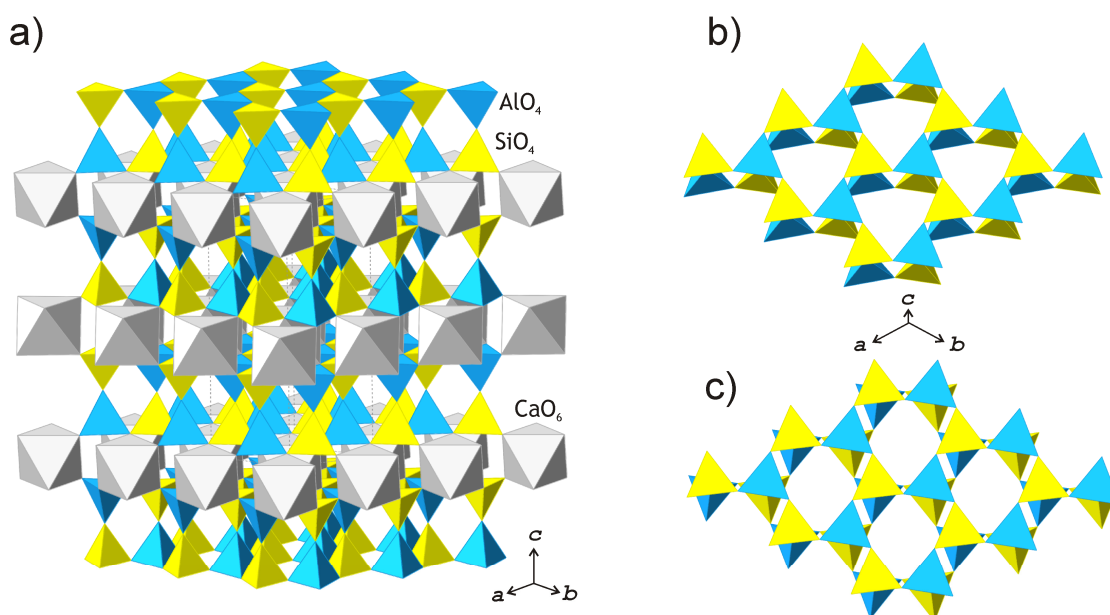


Figure 3. The crystal structure of dmisteinbergite (a) and views of the tetrahedral double layer when the O4 (b) and O4A (c) sites are occupied.

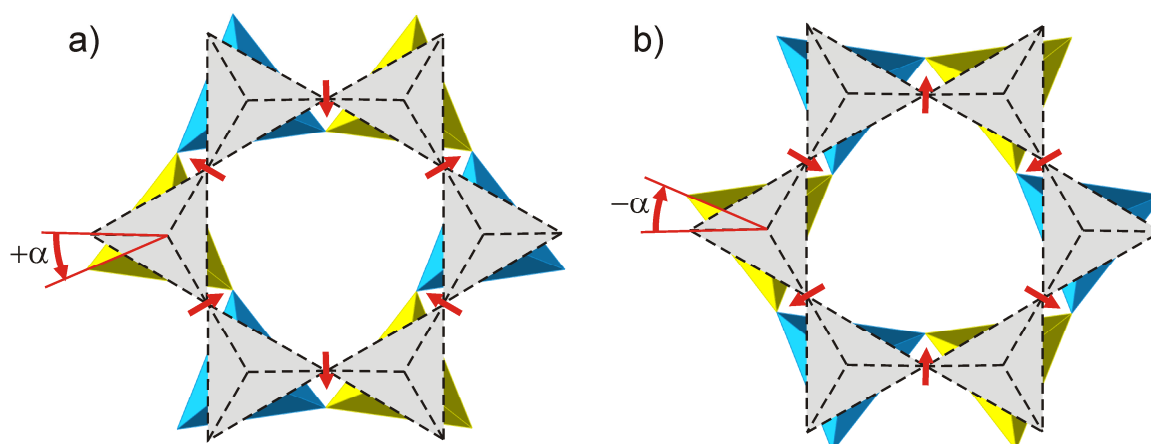


Figure 4. Ditrigonal rotation of tetrahedra in an ideal six-membered tetrahedral ring (gray tetrahedra with dashed outlines) results in two different versions of distorted ring with positive (a) and negative (b) values of the α angle. Red arrows indicate directions of shifts of bridging O atoms from their ideal positions.

The disorder of the O4 site also has a direct influence on the geometry of the interlayer space and coordination of the Ca atoms. There are two independent Ca sites in the crystal structure of dmisteinbergite. Coordination of the Ca1 site is not influenced by the disorder and is trigonal antiprismatic (distorted octahedral) (Figure 5b). In contrast, the coordination environment of the Ca2 site includes O4 and O4A atoms, and therefore, depends on the occupancies of the disordered O sites. If one of the two sites is occupied in both upper and lower tetrahedral layers (e.g., O4–O4 and O4A–O4a), the coordination is trigonal antiprismatic (Figure 5b; the A-type interlayer). However, if the occupancies of the sites are different (e.g., if the O4 site is occupied in the upper layer and the O4A site is occupied in the lower layer), the coordination becomes trigonal prismatic (Figure 5a; the B-type interlayer). Ferraris and Ivaldi [51] noted that for mica-group minerals, polytypes with the A-type

interlayer are more stable than those with the B-type interlayer. It is also noteworthy that the value of the ditrigonal rotation angle α (22.1°) is in good agreement with the values reported for Ca-bearing micas that have Ca^{2+} cations as interlayer species. For instance, in the crystal structure of clintonite, $\text{Ca}(\text{Mg},\text{Al})_3(\text{Al}_3\text{SiO}_{10})(\text{OH})_2$, the α value is in the range of $23.1\text{--}24.9^\circ$ [52]. The typical value of α for the rock-forming micas is in the range of $7\text{--}9^\circ$ [50].

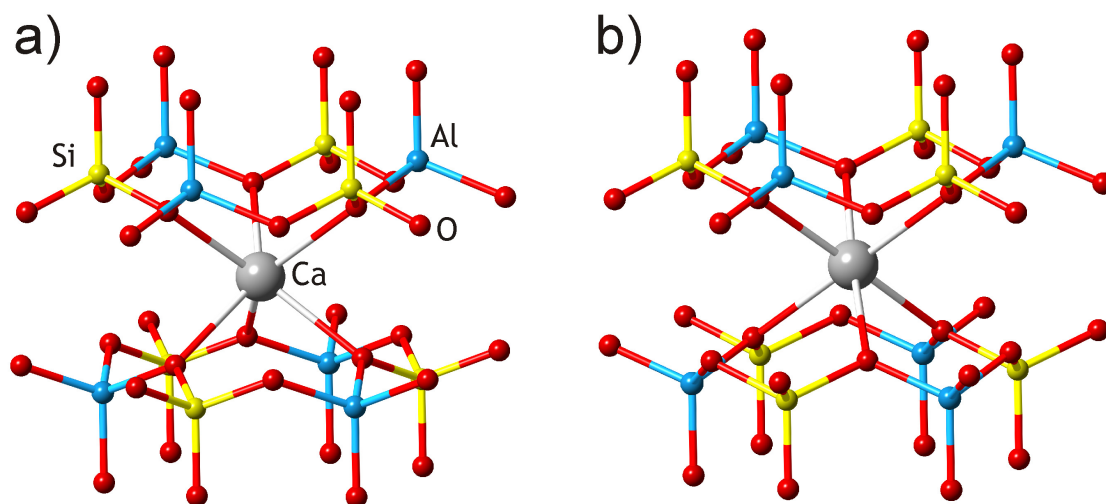


Figure 5. Two possible coordination environments of the Ca site in dmisteinbergite: trigonal prismatic (a) and trigonal antiprismatic (b) (distorted octahedral).

4. Discussion

The observed features of the crystal structure of dmisteinbergite from the type locality suggest the potential existence of different types of “hexagonal anorthite” that may differ in: (i) degree of disorder of the Al/Si tetrahedral sites, with completely disordered structure having the $P6_3/mcm$ symmetry; (ii) degree of disorder of the O sites (particularly O4 site), which have a direct influence upon the coordination of the Ca^{2+} cations (Ca2 site); (iii) polytypic variations (different stacking sequences and layer shifts). These features may explain, at least in part, the different symmetries reported for natural and synthetic dmisteinbergite [30,32,36,42]. It is interesting that the Raman spectra of dmisteinbergite crystals from different localities are slightly different, suggesting variable degrees of the Al/Si ordering by analogy with anorthite [53]. As was noted in a previous study [53], the peaks of symmetric bending vibrations of Si–O and Al–O bonds at 488 cm^{-1} for the most ordered anorthite species shifted to 485 cm^{-1} in shocked type anorthite and HT (high-temperature) anorthite. If this approach is used for the bands in the same range for dmisteinbergite spectra, then the sample from NWA 2086 meteorite should be more disordered dmisteinbergite (and sample from Katashina, Japan should be more ordered dmisteinbergite).

The formation of dmisteinbergite is usually associated with metastable crystallization in both natural [6,8,9,18–20] and synthetic [32–35,54–56] systems, indicating the kinetic nature of this phase. In the burned coal dumps, dmisteinbergite crystallizes directly from the gaseous phases together with the other metastable anorthite polymorph, svyatoslavite. Goldsmith [21] suggested that metastable, kinetically stabilized phases are usually structurally simpler than their stable counterparts. The complexity of crystal structures can be estimated using the information-based approach developed in previous studies [22,57]. The calculations of the structural complexity parameters for different anorthite polymorphs were performed using the TOPOSPRO software package [58] and the values are given in Table 6. It can be seen that the crystal structures of the metastable $\text{CaAl}_2\text{Si}_2\text{O}_8$ polymorphs dmisteinbergite and svyatoslavite are much simpler than that of anorthite, in good agreement with Goldsmith’s principle and similar previous observations [22–28,59,60].

Table 6. Information-based structural complexities of $\text{CaAl}_2\text{Si}_2\text{O}_8$ polymorphs and topological complexities of their tetrahedral units.

Polymorph	Topological Complexity of Tetrahedral Unit			Structural Complexity		
	v	I_G , bits/atom	$I_{G,total}$, bits/cell	v	I_G , bits/atom	$I_{G,total}$, bits/cell
anorthite	24	2.752	66.039	104	5.700	592.846
svyatoslavite	12	1.585	19.020	26	3.700	96.211
dmisteinbergite	12	1.459	17.510	26	3.046	79.192

It is also of interest to evaluate the topological complexity of aluminosilicate tetrahedral units in anorthite, dmisteinbergite, and svyatoslavite. The topological complexity is defined as the information-based complexity of the atomic arrangement with the highest possible symmetry. According to Baerlocher et al. [61], the tetrahedral framework in svyatoslavite corresponds to the BCT zeolite framework type with the $I4/mmm$ ideal space-group symmetry. The ideal symmetry of the double tetrahedral layer in dmisteinbergite is described by the subperiodic layer group $p6/mmm$. The ideal (topological) symmetry of the feldspar framework is $C2/m$ [62]. The information-based topological complexity parameters for the aluminosilicate units are given in Table 6, considering calculations of zeolite frameworks reported in a previous study [63]. It is evident that topological complexities of the tetrahedral units in three $\text{CaAl}_2\text{Si}_2\text{O}_8$ polymorphs are in agreement with Goldsmith's principle as well—kinetically stable but thermodynamically metastable phases are topologically simpler than thermodynamically stable ones. It is sometimes inferred that the formation of particular metastable polymorphs in aluminosilicate systems is determined by the structure of the initial melt [4]. However, this argument is not valid in our case, as the structures of the two metastable $\text{CaAl}_2\text{Si}_2\text{O}_8$ polymorphs are topologically different. In addition, crystallization from the gaseous phase does not involve any reasonable melting state. Therefore, we suggest that metastable crystallization in feldspar systems is a configurational entropy-driven process, where complexity is a major driving force as a parameter closely associated with the configurational entropy of atomic arrangements [64].

Supplementary Materials: The following are available online at <http://www.mdpi.com/2075-163X/9/10/570/s1>, Table S1: Anisotropic atom displacement parameters for dmisteinbergite, Dmisteinbergite.cif: Crystallographic Information file for the crystal structure of dmisteinbergite.

Author Contributions: Conceptualization, A.A.Z., V.V.G., and S.V.K.; methodology, A.A.Z., V.N.B., V.V.G., and S.V.K.; investigation, T.L.P., A.A.Z., M.A.R., and V.V.G.; writing—original draft preparation, A.A.Z., S.V.K., and T.L.P.; writing—review and editing, S.V.K. and A.A.Z.; visualization, A.A.Z., S.V.K., and T.L.P.

Funding: This study was supported by the Russian Foundation for Basic Research (the experimental part; grant No. 19-05-00628 to A.A.Z., V.V.G., T.L.P., and M.A.R.) and the Russian Science Foundation (the theoretical complexity analysis; grant No. 19-17-00038 to S.V.K.).

Acknowledgments: The experiments were carried out using facilities of the X-ray Diffraction and Geomodel Resource Centers of St. Petersburg University. Authors are grateful to Gregory Yu Ivanyuk (1966–2019) for the photograph of the dmisteinbergite specimen.

Conflicts of Interest: The authors declare no conflict of interest.

References

1. Yaroshevsky, A.A.; Bulakh, A.G. The mineral composition of the Earth's crust, mantle, meteorites, Moon, and planets. In *Advanced Mineralogy*; Marfunin, A.S., Ed.; Springer: Berlin/Heidelberg, Germany, 1994; Volume 1, pp. 27–36.
2. Ferrero, S.; Wunder, B.; Ziemann, M.A.; Wälle, M.; O'Brien, P.J. Carbonatitic and granitic melts produced under conditions of primary immiscibility during anatexis in the lower crust. *Earth Planet. Sci. Lett.* **2016**, *454*, 121–131. [CrossRef]

3. Ferrero, S.; Ziemann, M.A.; Angel, R.; O'Brien, P.J.; Wunder, B. Kumdykolite, kokchetavite and cristobalite crystallized in nanogranites from felsic granulites, Orlica-Snieznik Dome (Bohemian Massif): Not an evidence for ultrahigh pressure conditions. *Contrib. Mineral. Petrol.* **2016**, *171*, 3. [[CrossRef](#)]
4. Ferrero, S.; Angel, R. Micropetrology: Are inclusions in minerals grains of truth? *J. Petrol.* **2018**, *9*, 1671–1700.
5. Carvalho, B.B.; Bartoli, O.; Ferri, F.; Cesare, B.; Ferrero, S.; Remusat, L.; Capizzi, L.S.; Poli, S. Anatexis and fluid regime of the deep continental crust: New clues from melt and fluid inclusions in metapelitic migmatites from Ivrea Zone (NW Italy). *J. Metamorph. Geol.* **2019**, *37*, 951–975. [[CrossRef](#)]
6. Ma, C.; Krot, A.N.; Bizzarro, M. Discovery of dmisteinbergite (hexagonal $\text{CaAl}_2\text{Si}_2\text{O}_8$) in the Allende meteorite: A new member of refractory silicates formed in the solar nebula. *Am. Mineral.* **2013**, *98*, 1368–1371. [[CrossRef](#)]
7. Németh, P.; Lehner, S.W.; Petaev, M.I.; Buseck, P. Kumdykolite, a high-temperature feldspar from an enstatite chondrite. *Am. Mineral.* **2013**, *98*, 1070–1073. [[CrossRef](#)]
8. Fintor, K.; Walter, H.; Nagy, S. Petrographic and micro-Raman analysis of chondrules and (Ca, Al)-rich inclusions of NWA 2086 CV3 type carbonaceous chondrite. *Lunar Planet. Sci.* **2013**, *44*, 1152.
9. Fintor, K.; Park, C.; Nagy, S.; Pál-Molnár, E.; Krot, A.N. Hydrothermal origin of hexagonal $\text{CaAl}_2\text{Si}_2\text{O}_8$ (dmisteinbergite) in a compact type A CAI from the Northwest Africa 2086 CV3 chondrite. *Meteor. Planet. Sci.* **2014**, *49*, 812–823. [[CrossRef](#)]
10. Hwang, S.L.; Shen, P.; Chu, H.T.; Yui, T.F.; Liou, J.G.; Sobolev, N.V.; Zhang, R.Y.; Shatsky, V.S.; Zayachkovsky, A.A. Kokchetavite: A new polymorph of KAlSi_3O_8 from the Kokchetav UHP terrain. *Contrib. Mineral. Petrol.* **2004**, *148*, 380–389. [[CrossRef](#)]
11. Hwang, S.L.; Shen, P.; Chu, H.T.; Yui, T.-F.; Liou, J.G.; Sobolev, N.V. Kumdykolite, an orthorhombic polymorph of albite, from the Kokchetav ultrahigh-pressure massif, Kazakhstan. *Eur. J. Mineral.* **2009**, *21*, 1325–1334. [[CrossRef](#)]
12. Schertl, H.P.; Sobolev, N.V. The Kokchetav Massif, Kazakhstan: “Type locality” of diamond-bearing UHP metamorphic rocks. *J. Asian Earth Sci.* **2013**, *63*, 5–38. [[CrossRef](#)]
13. Liou, J.G.; Tsujimori, T.; Yang, J.; Zhang, R.Y.; Ernst, W.G. Recycling of crustal materials through study of ultrahigh-pressure minerals in collisional orogens, ophiolites, and mantle xenoliths: A review. *J. Asian Earth Sci.* **2014**, *96*, 386–420. [[CrossRef](#)]
14. Kotková, J.; Koda, R.; Machovi, V. Kumdykolite from the ultrahigh-pressure granulite of the Bohemian Massif. *Am. Mineral.* **2014**, *99*, 1798–1801. [[CrossRef](#)]
15. Perraki, M.; Faryad, S.W. First finding of microdiamond, coesite and other UHP phases in felsic granulites in the Moldanubian Zone: Implications for deep subduction and a revised geodynamic model for Variscan Orogeny in the Bohemian Massif. *Lithos* **2014**, *202*, 157–166. [[CrossRef](#)]
16. Di Pierro, S.; Gnos, E. Ca-Al-silicate inclusions in natural moissanite (SiC). *Am. Mineral.* **2016**, *101*, 71–81. [[CrossRef](#)]
17. Galuskina, I.O.; Galuskin, E.V.; Vapnik, Y.; Prusik, K.; Stasiak, M.; Dzierzanowski, P.; Murashko, M. Gurimite, $\text{Ba}_3(\text{VO}_4)_2$ and hexacelsian, $\text{BaAl}_2\text{Si}_2\text{O}_8$ —Two new minerals from schorlomite-rich paralava of the Hatrumim Complex, Negev Desert, Israel. *Mineral. Mag.* **2017**, *81*, 1009–1019. [[CrossRef](#)]
18. Nestola, F.; Mitterpergher, S.; Toro, G.D.; Zorzi, F.; Pedron, D. Evidence of dmisteinbergite (hexagonal form of $\text{CaAl}_2\text{Si}_2\text{O}_8$) in pseudotachylyte: A tool to constrain the thermal history of a seismic event. *Am. Mineral.* **2010**, *95*, 405–409. [[CrossRef](#)]
19. Mitterpergher, S.; Dallai, L.; Pennacchioni, G.; Renard, F.; Di Toro, G. Origin of hydrous fluids at seismogenic depth: Constraints from natural and experimental fault rocks. *Earth Planet. Sci. Lett.* **2014**, *385*, 97–109. [[CrossRef](#)]
20. Dobson, D.P.; Thomas, R.W.; Mitchell, T.M. Diffusion profiles around quartz clasts as indicators of the thermal history of pseudotachylytes. *Geochem. Geophys. Geosyst.* **2018**, *19*, 4329–4341. [[CrossRef](#)]
21. Goldsmith, J.R. A “simplexity principle” and its relation to “ease” of crystallization. *J. Geol.* **1953**, *61*, 439–451. [[CrossRef](#)]
22. Krivovichev, S.V. Structural complexity of minerals: Information storage and processing in the mineral world. *Mineral. Mag.* **2013**, *77*, 275–326. [[CrossRef](#)]
23. Cempírek, J.; Grew, E.S.; Kampf, A.R.; Ma, C.; Novák, M.; Gadas, P.; Škoda, R.; Vašinová-Galiiová, M.; Pezzotta, F.; Groat, L.A.; et al. Vránaite, ideally $\text{Al}_{16}\text{B}_4\text{Si}_4\text{O}_{38}$, a new mineral related to boralsilite, $\text{Al}_{16}\text{B}_6\text{Si}_2\text{O}_{37}$, from the Manjaka pegmatite, Sahatany Valley, Madagascar. *Am. Mineral.* **2016**, *101*, 2108–2117. [[CrossRef](#)]

24. Zaitsev, A.N.; Zhitova, E.S.; Spratt, J.; Zolotarev, A.A.; Krivovichev, S.V. Isolueshite, NaNbO_3 , from the Kovdor carbonatite, Kola peninsula, Russia: Composition, crystal structure and possible formation scenarios. *N. Jb. Mineral. Abh.* **2017**, *194*, 165–173. [[CrossRef](#)]
25. Krivovichev, S.V. Hydrogen bonding and structural complexity of the $\text{Cu}_3(\text{AsO}_4)(\text{OH})_3$ polymorphs (clinoclase, gilmarite): A theoretical study. *J. Geosci.* **2017**, *62*, 79–85. [[CrossRef](#)]
26. Krivovichev, S.V.; Hawthorne, F.C.; Williams, P.A. Structural complexity and crystallization: The Ostwald sequence of phases in the $\text{Cu}_2(\text{OH})_3\text{Cl}$ system (botallackite–atacamite–clinoatacamite). *Struct. Chem.* **2017**, *28*, 153–159. [[CrossRef](#)]
27. Plášil, J. Structural complexity of uranophane and uranophane- β : Implications for their formation and occurrence. *Eur. J. Mineral.* **2018**, *30*, 253–257. [[CrossRef](#)]
28. Huskić, I.; Novendra, N.; Lim, D.-W.; Topić, F.; Titi, H.M.; Pekov, I.V.; Krivovichev, S.V.; Navrotsky, A.; Kitagawa, H.; Friščić, T. Functionality in metal-organic framework minerals: Proton conductivity, stability and potential for polymorphism. *Chem. Sci.* **2019**, *10*, 4923–4929. [[CrossRef](#)]
29. Davis, G.L.; Tuttle, O.F. Two new crystalline phases of the anorthite composition, $\text{CaO-Al}_2\text{O}_3\text{-SiO}_2$. *Am. J. Sci. Bowen Volume.* **1951**, *1*, 107–114.
30. Takeuchi, Y.; Donnay, G. The crystal structure of hexagonal $\text{CaAl}_2\text{Si}_2\text{O}_8$. *Acta Crystallogr.* **1959**, *12*, 465–470. [[CrossRef](#)]
31. Takéuchi, Y.; Haga, N.; Ito, J. The crystal structure of monoclinic $\text{CaAl}_2\text{Si}_2\text{O}_8$: A case of monoclinic structure closely simulating orthorhombic symmetry. *Z. Kristallogr.* **1973**, *137*, 380–398.
32. Ito, J. High temperature solvent growth of anorthite on the join $\text{CaAl}_2\text{Si}_2\text{O}_8\text{-SiO}_2$. *Contrib. Mineral. Petrol.* **1976**, *59*, 187–194. [[CrossRef](#)]
33. Abe, T.; Tsukamoto, K.; Sunagawa, I. Nucleation, growth and stability of $\text{CaAl}_2\text{Si}_2\text{O}_8$ polymorphs. *Phys. Chem. Miner.* **1991**, *17*, 473–484. [[CrossRef](#)]
34. Abe, T.; Sunagawa, I. Hexagonal $\text{CaAl}_2\text{Si}_2\text{O}_8$ in a high temperature solution; metastable crystallization and transformation to anorthite. *Mineral. J.* **1995**, *17*, 257–281. [[CrossRef](#)]
35. Daniel, I.; Gillet, P.; McMillan, P.F.; Richet, P. An in-situ high-temperature structural study of stable and metastable $\text{CaAl}_2\text{Si}_2\text{O}_8$ polymorphs. *Mineral. Mag.* **1995**, *59*, 25–33. [[CrossRef](#)]
36. Dimitrijević, R.; Dondur, V.; Kremenović, A. Thermally induced phase transformations of Ca-exchanged LTA and FAU zeolite frameworks: Rietveld refinement of the hexagonal $\text{CaAl}_2\text{Si}_2\text{O}_8$ diphylosilicate structure. *Zeolites* **1996**, *16*, 294–300. [[CrossRef](#)]
37. Chesnokov, B.V.; Lotova, E.V.; Pavlyuchenko, V.S.; Nigmatulina, E.N.; Usova, L.V.; Bushmakin, A.R.; Nishanbaev, T.P. Svyatoslavite, $\text{CaAl}_2\text{Si}_2\text{O}_8$ (orthorhombic), a new mineral. *Zap. Vses. Mineral. Obshch.* **1989**, *118*, 111–114. (In Russian)
38. Krivovichev, S.V.; Shcherbakova, E.P.; Nishanbaev, T.P. The crystal structure of svyatoslavite and evolution of complexity during crystallization of a $\text{CaAl}_2\text{Si}_2\text{O}_8$ melt: A structural automata description. *Can. Mineral.* **2012**, *50*, 585–592. [[CrossRef](#)]
39. Chesnokov, B.V.; Lotova, E.V.; Nigmatulina, E.N.; Pavlyuchenko, V.S.; Bushmakin, A.F. Dmisteinbergite $\text{CaAl}_2\text{Si}_2\text{O}_8$ (hexagonal)-A new mineral. *Zap. Vses. Mineral. Obshch.* **1990**, *119*, 43–45. (In Russian)
40. Simakin, A.G.; Eremyashev, V.E.; Kucherinenko, Y.V. New data on dmisteinbergite. *Zap. Ross. Mineral. Obshch.* **2010**, *139*, 102–108. (In Russian)
41. Chesnokov, B.V.; Shcherbakova, E.P.; Nishanbaev, T.P. *Minerals from Burned Dumps of Chelyabinsk Coal Basin*; Institute of Mineralogy UrO RAS: Miass, Russia, 2008. (In Russian)
42. Akatsuka, K.; Yasumori, A.; Maeda, K. Structure of crystalline $\text{CaAl}_2\text{Si}_2\text{O}_8$ precipitated in a $\text{CaO-Al}_2\text{O}_3\text{-SiO}_2$ glass-ceramic. *Mater. Lett.* **2019**, *242*, 163–165. [[CrossRef](#)]
43. Bruker-AXS. *APEX2, Version 2014.11-0*; Bruker-AXS: Madison, WI, USA, 2014.
44. Sheldrick, G.M. *SADABS*; University of Goettingen: Goettingen, Germany, 2007.
45. Sheldrick, G.M. Crystal structure refinement with SHELXL. *Acta Crystallogr.* **2015**, *71*, 3–8.
46. Dolomanov, O.V.; Bourhis, L.J.; Gildea, R.J.; Howard, J.A.K.; Puschmann, H. Olex2: A complete structure solution, refinement and analysis program. *J. Appl. Crystallogr.* **2009**, *42*, 339–341. [[CrossRef](#)]
47. Brese, N.E.; O’Keeffe, M. Bond-valence parameters for solids. *Acta Crystallogr.* **1991**, *47*, 192–197. [[CrossRef](#)]
48. Lafuente, B.; Downs, R.T.; Yang, H.; Stone, N. The power of databases: the RRUFF project. In *Highlights in Mineralogical Crystallography*; Armbruster, T., Danisi, R.M., Eds.; W. De Gruyter: Berlin, Germany, 2015; pp. 1–30.

49. Pilz, W. Raman spectra of silicates. *Acta Phys. Hung.* **1987**, *61*, 27–30.
50. Brigatti, M.F.; Guggenheim, S. Mica crystal chemistry and the influence of pressure, temperature, and solid solution on atomistic models. *Rev. Mineral. Geochem.* **2002**, *46*, 1–97. [[CrossRef](#)]
51. Ferraris, G.; Ivaldi, G. Structural features of micas. *Rev. Mineral. Geochem.* **2002**, *46*, 117–153. [[CrossRef](#)]
52. Alietti, E.; Brigatti, M.F.; Poppi, L. Clintonite-1M: Crystal chemistry and its relationships to closely associated Al-rich phlogopite. *Am. Mineral.* **1997**, *82*, 936–945. [[CrossRef](#)]
53. Freeman, J.J.; Wang, A.; Kuebler, K.E.; Jolliff, B.L.; Haskin, L.A. Characterization of natural feldspars by Raman spectroscopy for future planetary exploration. *Can. Mineral.* **2008**, *46*, 1477–1500. [[CrossRef](#)]
54. Maeda, K.; Yasumori, A. Toughening of CaO–Al₂O₃–SiO₂ glass by dmisteinbergite precipitation. *Mater. Lett.* **2016**, *180*, 231–234. [[CrossRef](#)]
55. Maeda, K.; Yasumori, A. Nucleation and growth of hexagonal CaAl₂Si₂O₈ crystals in CaO–Al₂O₃–SiO₂ glass. *Mater. Lett.* **2017**, *206*, 241–244. [[CrossRef](#)]
56. Maeda, K.; Iwasaki, K.; Urata, S.; Akatsuka, K.; Yasumori, A. 3D microstructure and crack pathways of toughened CaO–Al₂O₃–SiO₂ glass by precipitation of hexagonal CaAl₂Si₂O₈ crystal. *J. Am. Ceram. Soc.* **2019**, *102*, 5535–5544. [[CrossRef](#)]
57. Krivovichev, S.V. Which inorganic structures are the most complex? *Angew. Chem. Int. Ed.* **2014**, *53*, 654–661. [[CrossRef](#)]
58. Blatov, V.A.; Shevchenko, A.P.; Proserpio, D.M. Applied topological analysis of crystal structures with the program package ToposPro. *Cryst. Growth. Des.* **2014**, *14*, 3576–3586. [[CrossRef](#)]
59. Izatulina, A.R.; Gurzhiy, V.V.; Krzhizhanovskaya, M.G.; Kuz'mina, M.A.; Leoni, M.; Frank-Kamenetskaya, O.V. Hydrated Calcium Oxalates: Crystal Structures, Thermal Stability and Phase Evolution. *Cryst. Growth Des.* **2018**, *18*, 5465–5478. [[CrossRef](#)]
60. Izatulina, A.R.; Gurzhiy, V.V.; Krzhizhanovskaya, M.G.; Chukanov, N.V.; Panikorovskii, T.L. Thermal Behavior and Phase Transition of Uric Acid and Its Dihydrate Form, the Common Biominerals Uricite and Tinnunculite. *Minerals* **2019**, *9*, 373. [[CrossRef](#)]
61. Baerlocher, C.; McCusker, L.B.; Olson, D.H. *Atlas of Zeolite Framework Types*, 6th ed.; Elsevier: Amsterdam, The Netherlands; London/Oxford, UK; New York, NY, USA; Paris, France; Tokyo, Japan, 2007.
62. Smith, J.V.; Brown, W.L. *Feldspar Minerals: 1. Crystal Structures, Physical, Chemical, and Microtextural Properties*, 2nd ed.; Springer: Berlin/Heidelberg, Germany; New York, NY, USA, 1988.
63. Krivovichev, S.V. Structural and topological complexity of zeolites: An information-theoretic analysis. *Micropor. Mesopor. Mater.* **2013**, *171*, 223–229. [[CrossRef](#)]
64. Krivovichev, S.V. Structural complexity and configurational entropy of crystals. *Acta Crystallogr.* **2016**, *72*, 274–276. [[CrossRef](#)]



© 2019 by the authors. Licensee MDPI, Basel, Switzerland. This article is an open access article distributed under the terms and conditions of the Creative Commons Attribution (CC BY) license (<http://creativecommons.org/licenses/by/4.0/>).